CCS Chemistry

RESEARCH ARTICLE

Received: Aug. 18, 2020 | Accepted: Oct. 5, 2020 | Published: Oct. 30, 2020

Molecular Tetrahedrons as Selective and Efficient Ion Transporters via a Two-Station Swing-Relay Mechanism

Ning Li[3], Jie Shen[3], Gerome Kusuma Ang[4], Ruijuan Ye[1,2] & Huaqiang Zeng[1,2]*

[1]Institute of Advanced Synthesis, Northwestern Polytechnical University, Xi'an, Shaanxi 710072, [2]Yangtze River Delta Research Institute, Northwestern Polytechnical University, Taicang, Jiangsu 215400, [3]The NanoBio Lab, The Nanos, Singapore 138669, [4]Raffles Institution, Singapore 575954

**Corresponding author: hqzeng@nwpu.edu.cn*

Cite this: *CCS Chem.* **2020**, *2*, 2269–2279

The traditional approach to utilizing an ion-relay mechanism for ion transport requires three or more ion-relay stations. Herein, we describe a novel strategy, incorporating a swing action to realize a minimal ion-relay mechanism via only two relay stations. This swing-relay mechanism was achieved using a class of crown ether-appended, long-armed molecular tetrahedrons (MTs). These MTs comprise ion-relaying crown units attached to a rigid tetrahedral core via flexible alkyl linkers, which act as the mobile arms and endow the crown units with great mobility to swing. Driven by the ionic concentration gradient and supported by the mobile arms, two crown units located in the membrane's opposite hydrophilic regions swing toward each other to complete a single ion-relay step in the center of the membrane to enable fast ion conduction across. Generally, 18-crown-6-containing MT6s exhibited higher activities and better K^+/Na^+ selectivities than 15-crown-5-containing MT5s, with the most active MT6-C10 displaying an EC_{50} (K^+) of 0.9 μM (i.e., 0.9 mol % relative to lipid) and the most selective MT6-C4 showing K^+/Na^+ selectively of 6.3. Finally, five control MTs were rationally designed to establish the action of the novel unimolecular two-station swing-relay as an efficient yet unprecedented mechanism of synthetic ion transporters.

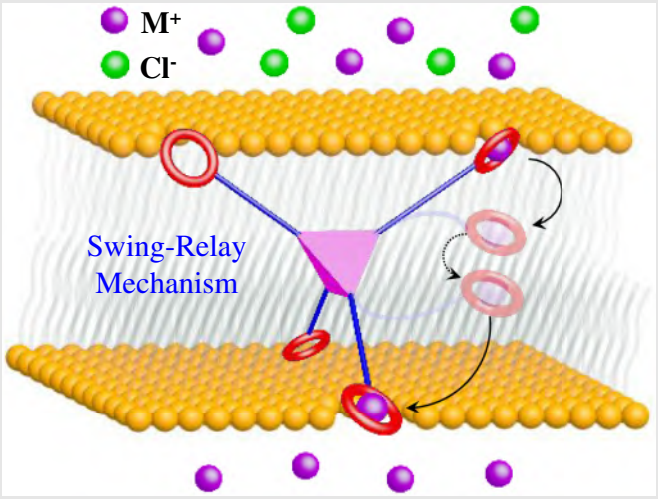

Keywords: **supramolecular chemistry, artificial membrane transporters, ion-relay mechanism, crown ethers**

Introduction

Precisely regulated ion flow across the cell membrane plays a crucial role in numerous biological processes, and thus, the perturbation of this process is closely associated with many physiological disorders and subsequent human diseases.[1,2] Understanding how the naturally evolved ion transporters function and designing artificial

DOI: 10.31635/ccschem.020.202000475
Citation: *CCS Chem.* **2020**, 2, 2269–2279
Citation denotes calendar and volume year of first online publication.
Issue Assignment: Volume 3 (2021), Issue 8

versions of comparable or even exceeding performance have attracted extensive worldwide research interest due to their scientific significance and great potential in the biomedical marketplace.[3-8]

Passive transmembrane transport of ions is mainly accomplished by channel- or carrier-mediated mechanisms, in which ions pass through the membrane via a preformed passage spanning across or via reversible binding with ionophores mobilized in the lipid bilayer.[9-25] The cross-membrane ion transporters, which do not use a conventional channel or carrier mechanisms, are an exciting class of artificial membrane transporters and to date remain largely unexplored, with only a few reports available in the open literature.[26-29]

In 2018, Chen et al.[27] reported a rotaxane-derived molecular shuttle for K^+ ion transportation, with an EC_{50} (K^+) value equivalent to 3 mol % of lipid present. Featuring the molecular machine concept with much simpler molecular

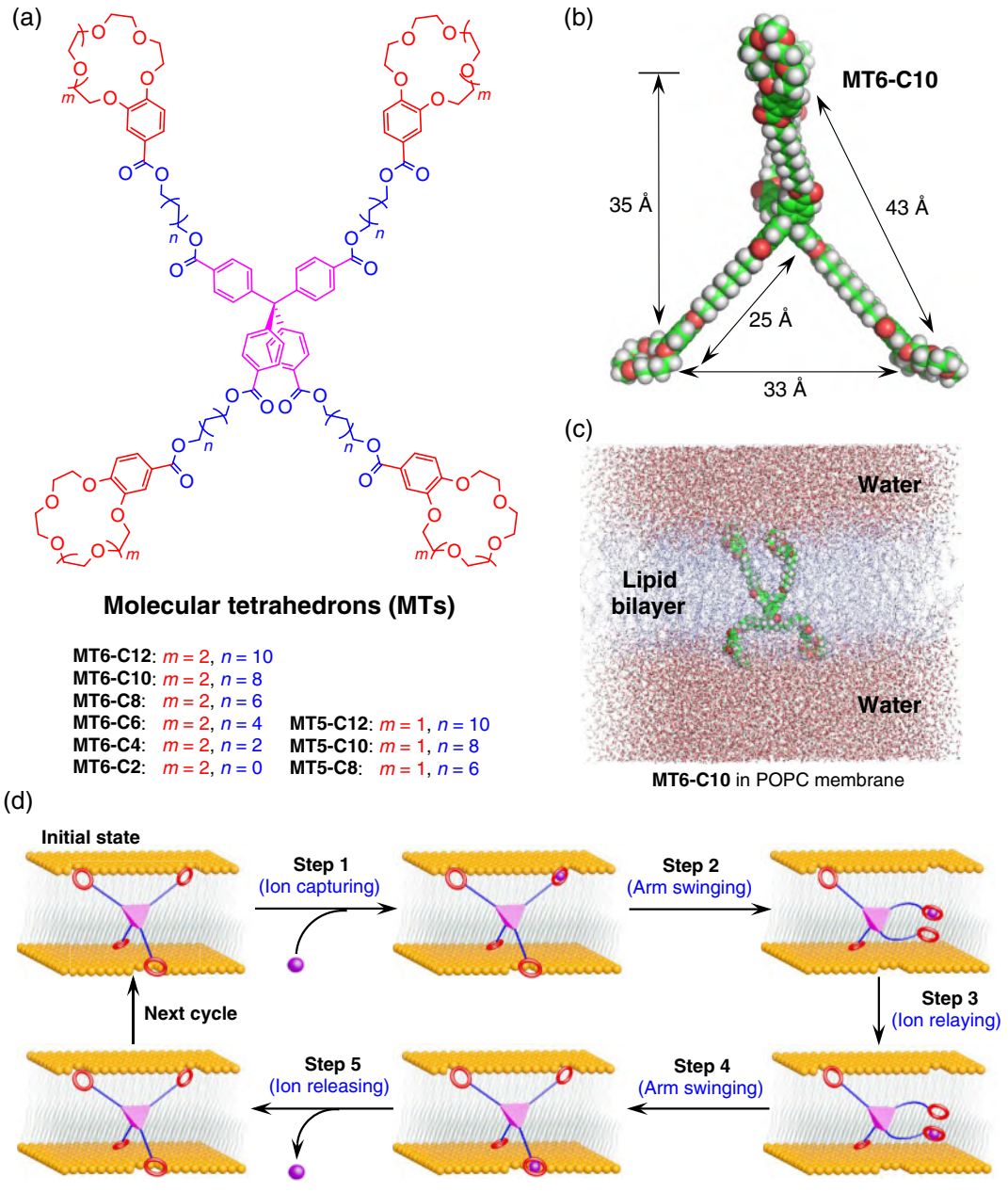

Figure 1 | *(a) General chemical structure of the **MT**s. (b) Computationally optimized structure of **MT6-C10** at the ωB97X/6-31G* level and its physical dimension from the CPK model. (c) Side-view snapshot of MD-simulated configuration of **MT6-C10** in lipid bilayer membrane surrounded by an aqueous environment. (d) Schematic illustration of the proposed two-station swing-relay mechanism involving a head-to-head meet of two crown units for ion relay in the center of the membrane. **MT**s, molecular tetrahedron; CPK, Corey–Pauling–Koltun; MD, molecular dynamics.*

DOI: 10.31635/ccschem.020.202000475
Citation: *CCS Chem.* **2020**, 2, 2269–2279
Citation denotes calendar and volume year of first online publication.
Issue Assignment: Volume 3 (2021), Issue 8

designs, two alternative highly active synthetic ion transporters were also demonstrated very recently, namely molecular swing[28] and molecular ion fisher[29] that facilitate ion transport by swinging and fishing actions, respectively. Although both molecular swings and ion fishers share certain structural similarities, they differ vastly in their ion transport activities and selectivities, foreshadowing the versatile potential of structurally fine-tuned swings and fishers in the field of synthetic ion transporters.

A conventional ion-relay mechanism for ion transport requires three or more relay stations to fully span the hydrophobic membrane region, with at least one station residing around the center of the membrane where ions experience the highest energetic penalty.[18,30–37] During the ion-relay process, where the preceding station captures and relays the ion to the next station, all stations do not move significantly. We envisioned that the number of relay stations could be reduced to two if they are customized to be capable of swinging along the membrane axis back and forth between the membrane's hydrophilic region and its center.[26] In this work, we disclose a unique class of crown ether-appended tetrahedron-shaped ion transporters called molecular tetrahedrons (**MT**s) (Figures 1a–1c), which are indeed appropriately sized to enable highly efficient ion transport via a swing-relay mechanism minimally mediated by just two ion-relay stations and a single ion-relay step (Figure 1d). The modularly designed nanosized **MT**s consisted of a rigid tetrahedral core, flexible alkyl linkers of appropriate lengths, and ion-relaying crown ether units at the tetrahedron vertices. With the tetrahedron core serving as the anchor and the flexible linkers as the rope (Figures 1b and 1c), the peripheral crown ether-based relay stations become capable of swinging, relaying, and eventually conducting ions across lipid membranes (Figure 1d). Such a unique molecular design, incorporating three-dimensional (3D)-shaped mobile arms provides a novel approach and a new ion-relay principle to construct highly efficient ion transporters toward interesting applications relative to membrane transport.

Experimental Methods

Synthesis of MTs

In this study, **MT**s were prepared via a dual-step synthetic procedure, exemplified by the preparation of **MT6-C10** in the following discussion. First, a suspension of 1,10-dibromodecane (3.00 g, 10 mmol), 4′-carboxybenzo-18-crown-6 (356 mg, 1.0 mmol), and potassium carbonate (276 mg, 2.0 mmol) in acetonitrile (20 mL) was heated at 85 °C overnight. Removal of the solvent in vacuo gave the crude product, purified by flash column chromatography using ethyl acetate to afford the pure tetrahedron arm product purified by preparative thin layer chromatography (silica gel layer, 20 cm × 20 cm (L × W), 1 mm in gel thickness).[29] Then a suspension of the prepared tetrahedron arm (201 mg, 0.34 mmol), potassium carbonate (96.7 mg, 0.70 mmol), and a 4,4′,4″,4‴-methanetetrayltetrabenzoic acid (34.7 mg, 0.070 mmol) was dissolved in anhydrous dimethylformamide (10 mL) and heated to 100 °C overnight. Next the reaction mixture was filtered to obtain a clear orange solution. Removal of the solvent in vacuo gave the crude product, which was purified by preparative thin-layer chromatography using methanol/dichloromethane (8/100) to afford a pure pale yellow solid product of **MT6-C10**. All other **MT**s were synthesized using similar procedures. Synthesis and characterization details are found in Supporting Information Figure.

Molecular dynamic simulation

A membrane builder in CHARMM-GUI was used to build the initial protein/membrane complex structure. The protocol comprised six steps, sequentially performed in the following order: objects reading, objects orientation, system size determination, building a lipid bilayer, assembling lipid bilayer, and system equilibrium. The **MT6-C10** molecule was placed in the center of the membrane made up of 256 phosphatidylcholine (POPC) molecules, with the removal of lipid molecules within 1 Å from the **MT6-C10** molecules. Then the membrane was placed in a box with dimensions of 93 × 93 Å in width and 99 Å in height. Subsequently, 15,061 water molecules were placed on the top and bottom sides of the membrane (~ 7500 on each side) for each system. Counter KCl ions were added to produce an ion concentration of 0.15 M. During molecular dynamics (MD) simulations, the pressure was maintained at 1 bar. After equilibration steps, the simulation's production run was performed for 100 ns, and the structure at the 100th ns trajectory was used for analyzing the orientation of the **MT6-C10** molecule. Further details are presented in Supporting Information Figure.

8-Hydroxypyrene-1,3,6-trisulfonic acid assay to evaluate ion transport performance

Egg yolk l-α-phosphatidylcholine (EYPC; 1.0 mL, 25 mg/mL in $CHCl_3$; Avanti Polar Lipids, Alabaster, AL) was loaded in a round-bottom flask, and the solvent was removed under reduced pressure at 30 °C. The resultant film was dried under high vacuum overnight at room temperature and hydrated with 4-(2-hydroxyethyl)-1-piperazine-ethane sulfonic acid (HEPES) buffer solution (1.0 mL, 10 mM HEPES, 100 mM NaCl, pH = 7.0) containing a pH-sensitive dye 8-hydroxypyrene-1,3,6-trisulfonic acid (HPTS; 1.0 mM) at room temperature for 45 min to give a milky suspension. Then the mixture was subjected to 10 freeze–thaw cycles: freezing in liquid N_2 for 1 min

DOI: 10.31635/ccschem.020.202000475
Citation: *CCS Chem.* **2020**, 2, 2269–2279
Citation denotes calendar and volume year of first online publication.
Issue Assignment: Volume 3 (2021), Issue 8

and heating at 55 °C in a water bath for 2 min. The vesicle suspension was extruded through polycarbonate membrane (0.1 μm) to produce a homogeneous suspension of large unilamellar vesicles (LUVs) of ~120 nm in diameter with HPTS encapsulated inside. The extravesicular HPTS dye was separated from the LUVs using size-exclusion chromatography (stationary phase: Sephadex G-50, GE Healthcare, Smyrna, GA; mobile phase: 10 mM HEPES buffer with 100 mM NaCl). The mobile phase was diluted to yield an LUV stock solution of 5.0 mL of 6.5 mM and stored at a 4 °C refrigerator until use.

The HPTS-containing LUV suspension (30 μL, 6.5 mM in 10 mM HEPES buffer containing 100 mM NaCl at pH = 7.0) was added to a HEPES buffer solution (1.96 mL, 10 mM HEPES, 100 mM MCl at pH = 8.0, where $M^+ = Li^+$, Na^+, K^+, Rb^+, and Cs^+) to create a pH gradient for ion transport study. Then a solution of **MT**s or control compounds in dimethyl sulfoxide (DMSO) was injected into the suspension under gentle stirring. Upon addition, the emission of HPTS was monitored immediately at 510 nm with excitations at both 460 and 403 nm, recorded simultaneously for 300 s using a fluorescence spectrophotometer (Model F-7100; Hitachi, Tokyo, Japan). At $t = 300$ s, an aqueous solution of Triton X-100 (20 μL, 20% v/v) was injected to induce a maximum change in dye fluorescence emission. The final transport trace was obtained as a ratiometric value of I_{460}/I_{403} and normalized based on the ratiometric value of I_{460}/I_{403} after the addition of Triton using the equation $I_f = [(I_t - I_0)/(I_1 - I_0)]$, where I_f = fractional emission intensity, I_t = fluorescence intensity at time t, I_1 = fluorescence intensity after the addition of Triton X-100, and I_0 = initial fluorescence intensity. The fractional change R_{M^+} was calculated for each curve using the normalized value of I_{460}/I_{403} at 300 s before the addition of Triton, with the ratio of a blank set as 0 and that of Triton as 1. By fitting the fractional transmembrane activity, R_{M^+}, versus transporter concentration using the Hill equation: $Y = 1/(1 + (EC_{50}/[C])^n)$, we obtained the EC_{50} values and Hill coefficient n.

CF dye leakage assay

LUVs containing 5(6)-carboxyfluorescein dyes were prepared via similar procedures with that in the HPTS assay, except for the hydration step, wherein the lipid film was hydrated with HEPES buffer solution (1.0 mL, 10 mM HEPES, 100 mM NaCl, pH = 7.5) containing 5(6)-fluorescein (CF; 50 mM) at room temperature for 45 min. Details are presented in Supporting Information Figure S24. Then the CF-containing LUV suspended in LUV buffer (30 μL, 6.5 mM in 10 mM HEPES buffer containing 100 mM NaCl at pH = 7.5) was added to a HEPES buffer solution (1.96 mL, 10 mM HEPES, 100 mM NaCl at pH = 7.5) to create a concentration gradient for the CF dye transport study. A solution of **MT6-C10** (3.5 μM) or natural pore-forming peptide melittin in DMSO at different concentrations was then injected into the suspension under gentle stirring. Upon adding **MT**s or pore-forming peptide molecules, the emission of the CF dye was monitored immediately at 517 nm with excitations at 492 nm for 300 s. At $t = 300$ s, an aqueous solution of Triton X-100 (20 μL, 20% v/v) was added immediately to destroy the CF dye gradient completely.

Results and Discussion

Molecular design and synthesis

In designing **MT** ion transporters, a few criteria were borne in mind, including (1) specific functional groups for selective ion capturing, (2) the movable and lipid-compatible moieties for ion transportation, and (3) appropriate physical dimension that would span across the entire membrane lipid bilayer. In the literature, crown ethers have been widely reported on their binding affinity to alkali metal ions,[38,39] and have frequently been utilized in constructing ion transporters,[18,19,33–37] thereby representing a good option as the selective ion-capturing group. We accomplished the synthesis of MTs by reacting 4-carboxybenzo-crown ether with dibromoalkane of appropriate lengths to construct the tetrahedron arm first, followed by reacting the arm with a 4,4′,4″,4‴-methanetetrayltetrabenzoic acid as the tetrahedral core to establish the desired tetrahedron configuration (Figure 1a and Supporting Information Scheme S1). The flexible alkyl chain was selected primarily because of its structural simplicity and flexibility, as well as its excellent compatibility with the hydrophobic lipid tails in the membrane. Via this facile dual-step synthetic scheme, six-related **MT**s were modularly prepared using three types of alkyl linkers (*n*-C_8H_{16}, *n*-$C_{10}H_{20}$, and *n*-$C_{12}H_{24}$) and two classes of crown units (18-crown-6 and 15-crown-5; Figure 1a). These compounds were characterized by ^1H and ^{13}C NMR spectra and high-resolution mass spectra (see Supporting Information Figure S25–S42 for more details).

As an example of the **MT** family, the computationally optimized molecular structure of **MT6-C10**, containing 18-crown-6 units and *n*-$C_{10}H_{20}$ linkers, agreed with the expected tetrahedron configuration (Figure 1b). The distance between the opposite tetrahedron edges, excluding the crown units was calculated to be 35 Å at its most extended state, according to the Corey–Pauling–Koltun (CPK) model. The distances were 32 and 38 Å for **MT6-C8** and **MT6-C12**, respectively. All these values were comparable with the typical thickness of the membrane hydrophobic region, hence, confirming the appropriate physical dimension of these **MT**s to span across the bilayer membrane. To further validate the molecular design, MD simulation of an all-atom **MT6-C10** model in the lipid bilayer, performed for 100 ns in an aqueous environment. The stabilized snapshot revealed a favorable

DOI: 10.31635/ccschem.020.202000475
Citation: *CCS Chem.* **2020**, 2, 2269–2279
Citation denotes calendar and volume year of first online publication.
Issue Assignment: Volume 3 (2021), Issue 8

configuration of **MT6-C10** sandwiched in the membrane, with two crown ethers at the top membrane–water interface and the other two at the bottom (Figure 1c). Considering the alkyl linker's structural flexibility and crown ether's ion binding affinity, these rationally designed **MT**s might perform as efficient ion transporters to move cations across the membrane in the presence of an ionic concentration gradient.

A hypothetical swing-relay mechanism for ion transport

In view of the unique tetrahedral molecular design, we hypothesized that the ion transport is dominated by an unconventional swing-relay mechanism that employs two of the four crown units, one from the top and one from bottom side, to transport a cation across the membrane. The step-by-step illustration of the proposed swing-relay action is shown in Figure 1d. The critical step involves a head-to-head meet of two ion-binding crown units at the central membrane line, where the highest energetic penalty for cations resides. Starting from the MD-simulated configuration as the initial state, one of the crown ethers at the top membrane–water interface first captures an ion (Step 1, Figure 1d). Driven by the ionic concentration gradient, this ion-carrying arm swings toward the membrane center (Step 2, Figure 1d). When it meets another arm that also swings stochastically toward the membrane center, ion-relay takes place between the two vicinal crown ethers (Step 3, Figure 1d). The ionic gradient further drives the new ion-carrying arm to swing back to its more extended state (Step 4, Figure 1d), followed by ion release (Step 5, Figure 1d). Subsequently, the system returns to the initial state to start the next swing-relay cycle. In this process, each of the two operational arms, on average, must only carry the ion across no more than half of the hydrophobic membrane region. Therefore, it should be of much higher efficiency than the

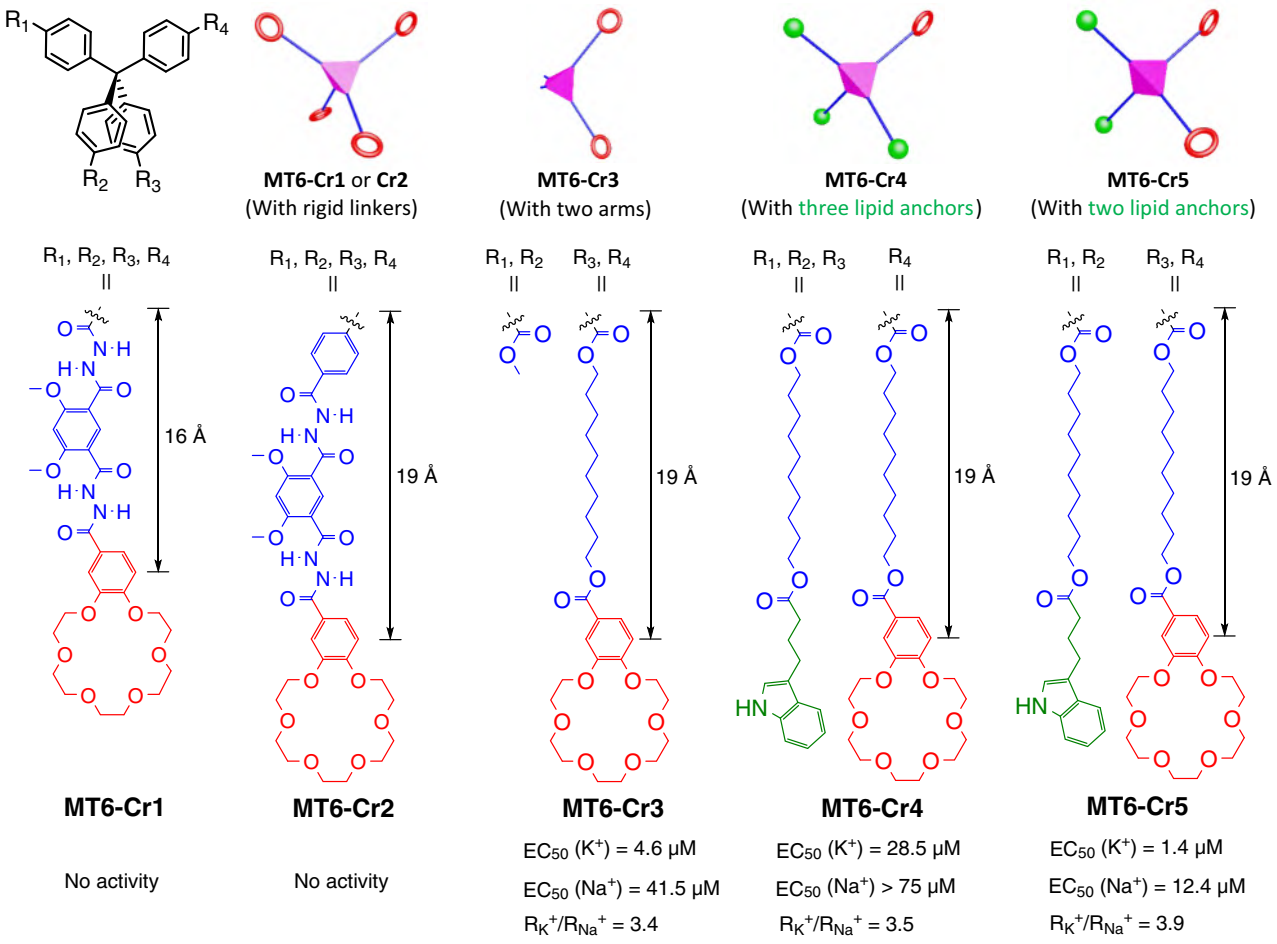

Figure 2 | *Molecular design of the control compounds **MT6-Cr1** and **MT6-Cr2** with rigid linkers linearly locked by intramolecular H-bonding, **MT6-Cr3** that only contains two operational mobile arms, **MT6-Cr4** featuring three indolyl-containing arms in green as lipid anchors and only a single mobile 18-crown-6-containing arm, and **MT6-Cr5** with two indolyl-containing lipid anchors and two mobile 18-crown-6-containing arms. Note that in terms of physical dimensions, **MT6-Cr1** is almost identical to **MT6-C6**, and **MT6-Cr2** to **MT6-Cr5** are almost identical to **MT6-C10**.*

DOI: 10.31635/ccschem.020.202000475
Citation: *CCS Chem.* **2020**, 2, 2269–2279
Citation denotes calendar and volume year of first online publication.
Issue Assignment: Volume 3 (2021), Issue 8

other possibility of nonrelaying swing-only transport, in which a single-arm carries the ion across the entire membrane width, as described later with **MT6-Cr4** (Figure 2). It is also worth emphasizing that both crown units at the top membrane–water interface are active for ion capturing, and they can convey their captured ions to either of the crown ethers at the bottom. In other words, there exist four equivalent active ion-relay pathways.

To validate the swing-relay proposition, specific control **MT** compounds were designed and prepared, mainly with a focus on (1) verifying the indispensable role of structural flexibility of **MT** linkers, (2) confirming the synergistic effect among the mobile tetrahedron arms, and (3) probing the role played by the alternative nonrelaying swing-only in ion conduction (see Figure 2 and later discussions).

High ion transport activity by MT6s

Ion transport activities of these **MT**s were evaluated experimentally using the well-established HPTS assay constructed upon LUVs (Figure 3a), with an extravesicular environment of 100 mM MCl (M^+ = Li^+, Na^+, K^+, Rb^+, and Cs^+) at pH 8.0. The intravesicular region contains 100 mM NaCl and 1.0 mM pH-sensitive HPTS dye at pH 7.0. Driven by the pH gradient, cross-membrane ion transport is always coupled with an intravesicular pH change that can be monitored macroscopically by the HPTS fluorescence intensity.

Using the HPTS assay, we found that **MT6**s transport K^+ ions much faster than other alkali metal ions, with **MT6-C10** exhibiting the highest fractional K^+ transport activity of 100% at 3.5 μM (Figure 3b). The ion selectivity follows the order $K^+ > Rb^+ > Na^+ > Cs^+ > Li^+$ (Figure 3c and Supporting Information Figure S1), which agrees with the Eisenman sequence IV.[40] This suggests that the observed selectivity could be ascribed to ion recognition by the crown units instead of ion dehydration energy or ionic radius. Interestingly, most **MT5**s transport Na^+ faster than the other cations, following the order $Na^+ \geq K^+ > Rb^+ > Li^+ > Cs^+$, and the best performer, **MT5-C12**, exhibiting a fractional activity of 85.2% at 40 μM (see Supporting Information Figure S2).

Then we performed Hill analyses to determine the EC_{50} values of these **MT**s in transporting K^+ and Na^+ ions, which are most relevant to physiological settings (see Supporting Information Figures S3–S8). The ion transport selectivity can also be quantified by simply taking the reciprocal ratio of the EC_{50} values. In general, **MT6**s exhibited both high activity (EC_{50} = 0.9–1.6 μM for K^+, corresponding to 0.9–1.6 mol % relative to lipid) and likely excellent K^+/Na^+ selectivity [$EC_{50}(Na^+)/EC_{50}(K^+)$ = 7.1–15.3] (Table 1). However, this EC_{50}-based selectivity might be inaccurate in situations where the transporters are poorly soluble or interact unfavorably with the membrane. In this regard, we recently proposed the use of R_K^+/R_{Na}^+ ratio (see Supporting Information for details) as an alternative yet reliable index for evaluation of ion transport selectivity (Figure 3c and Table 1), provided that the normalized fractional fluorescence intensity R_M^+ is obtained at the transporter concentration where the transport activity for the most active ion reaches > 90% over the 300 s data recording period.[29] Recently, the reliability of using such R_M^+ ratios to derive

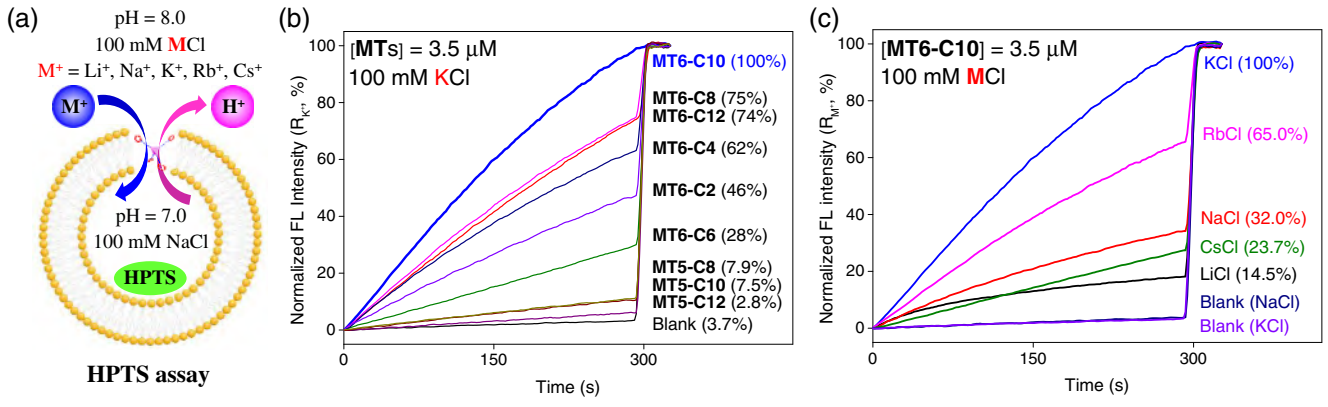

Figure 3 | *(a) Schematic illustration of the pH-sensitive HPTS assay for the ion transport study. Different extravesicular salts are used to facilitate the comparison of ion transport activities. (b) Fractional K^+ transport activities of various **MT**s determined over 300 s at 3.5 μM. The normalized fluorescence intensity R_K^+ is calculated using the formula $R_K^+ = (I_K^+ - I_O)/(I_{Triton} - I_O)$, in which I_K^+ and I_{Triton} are the values of the $I_{460\ nm}/I_{403\ nm}$ ratio at 300 s before and after the triton addition, respectively, and I_O is the background intensity. (c) M^+ ion transport selectivity of the most active K^+-transporting **MT6-C10**, determined > 300 s at 3.5 μM with an extravesicular environment of 100 mM MCl (M^+ = Li^+, Na^+, K^+, Rb^+, and Cs^+). [Total lipid] = 97.5 μM. HPTS, 8-hydroxypyrene-1,3,6-trisulfonic acid; **MT**s, molecular tetrahedron.*

DOI: 10.31635/ccschem.020.202000475
Citation: *CCS Chem.* **2020**, 2, 2269–2279
Citation denotes calendar and volume year of first online publication.
Issue Assignment: Volume 3 (2021), Issue 8

Table 1 | *Experimentally Determined EC_{50} (μM), EC_{50} (Na^+)/EC_{50} (K^+), and R_K^+/R_{Na}^+ Values for* ***MT****s*

	MT5-C12	MT5-C10	MT5-C8	MT6-C12	MT6-C10	MT6-C8	MT6-C6	MT6-C4	MT6-C2[c]
EC_{50} (Na^+)[a]	8.8 ± 0.3	23.5 ± 2.2	40.1 ± 1.7	11.3 ± 0.3	13.1 ± 0.4	21.4 ± 0.3	45.4 ± 1.3	>32	—
EC_{50} (K^+)[a]	>40	36.6 ± 2.5	37.3 ± 0.8	1.6 ± 0.1	**0.9 ± 0.1**	1.4 ± 0.1	9.0 ± 0.8	1.8 ± 0.1	3.8 ± 0.2
$\frac{EC_{50}(Na^+)}{EC_{50}(K^+)}$	<0.2	0.6	1.1	7.1	14.6	15.3	5.0	>17.8	—
R_K^+/R_{Na}^+[b]	0.4	0.7	1.1	2.5	3.1	3.3	1.9	**6.3**	—

Note: HPTS, 8-hydroxypyrene-1,3,6-trisulfonic acid. Bold values refer to the most active and most selective molecular tetrahedrons.
[a] [Total lipid] = 97.5 μM.
[b] See Supporting Information Figure S1–S11 for more details.

ion transport selectivity has also been verified by Zeng et al.[41] Using this index, all **MT6**s were still found to be K^+ selective, with the K^+/Na^+ selectivity falling in the range of 2.5–3.3 (Table 1). In comparison, **MT5-C12**, being the most active in the Na^+-selective **MT5**s family, showed an $EC_{50}(Na^+)$ value of 8.8 μM and a Na^+/K^+ selectivity of 2.2.

We elucidated the additional impact of the alkyl linker length toward ion transport properties of the better performing **MT6**s series by synthesizing three additional **MT6**s with shorter linkers (i.e., **MT6-C6**, **MT6-C4**, and **MT6-C2**) and assessed their ion transport performance using the same pH-sensitive HPTS assay. While all of them demonstrated K^+ selectivity and generally highly active, their ion transport activities were inferior to that of **MT6-C10** and did not monotonously decrease with alkyl linker length (Table 1). Given the sandwich-like configuration in the lipid bilayer (Figure 1c), some **MT6**s of intermediate size might have possessed the most appropriate physical dimension to have their crown units most stably docked at the membrane–water interfaces to attenuate the ability to swing. This would make the arm curling energetically less favorable, compared with other longer or shorter ones, and hence, largely sabotage their ion transport ability. Experimentally, we identified one such special case to be **MT6-C6**, which exhibited a much lower K^+ transport activity [$EC_{50}(K^+) = 9.0$ μM] than the other five **MT6**s [EC_{50} (K^+) = 0.9–3.8 μM, Table 1]. The alkyl linker length also imposed a significant influence on the ion transport selectivity. Using the aforementioned R_M^+ ratio-based approach, a good K^+/Na^+ selectivity of 6.3 was determined for **MT6-C4**, which stood out from the rest of **MT6** members ($R_K^+/R_{Na}^+ = 1.9$–3.3). The K^+/Na^+ selectivity of this most selective **MT6-C4** and also the most active **MT6-C10** in the **MT6**s family was also verified qualitatively by the membrane potential experiments with Safranin O (see Supporting Information Figure S12 for details). Similar linker length dependency of ion transport activity and selectivity was also observed for the **MT5**s, although their overall performances were poor (Table 1).

Transport mechanism study

Further, we prepared a group of structurally related yet functionally specific control **MT**s to show that it is the swing-relay action of the flexible arms that accounts for highly efficient ion transport performance.

First, since the ion-relaying action depends largely on the arm curling/swinging to facilitate the head-to-head meet of crown units, we envisioned that similar-sized **MT**s with rigid arms, which can only undergo minimal movement via limited covalent bond rotation in the membrane, are incapable of transporting K^+ or Na^+ ions, regardless of their arm lengths. To this end, we prepared two control **MT**s, namely **MT6-Cr1** and **MT6-Cr2**, by replacing the flexible alkyl linkers with rigid ones, which were locked linearly by intramolecular hydrogen bonding (Figure 2). These controls possess almost identical physical dimensions to those of **MT6-C6** and **MT6-C10** and could readily span across the lipid membrane, but as expected, it turned out to elicit negligible Na^+ or K^+ transport activities experimentally, even at concentrations as high as 10 μM (see Supporting Information Figure S13). The lack of detectable activities of **MT6-Cr1** and **MT6-Cr2** pointed further to a limited contribution to ion transport by simple molecular rotation, much like a windmill. It is worth mentioning that only **MT6-Cr2** with a rigid linker showed visible precipitates by naked eyes among all **MT**s and the control compounds tested at 10 μM, with the UV–vis measurement revealing at least 50% **MT6-Cr2** incorporation into LUVs at 10 μM (see Supporting Information Figure S14). This further suggests that >50% of other soluble tetrahedrons might have been incorporated into LUVs. In situ dynamic light scattering (DLS) measurements were carried out to monitor the formation of precipitates of the rigidly armed **MT6-Cr1** and **MT6-Cr2** at varying concentrations in the LUV buffer. As shown in Supporting Information Figure S15, the addition of **MT6-Cr1** into the LUV buffer with concentrations up to 10 μM did not produce any precipitates, indicating that all of the compounds penetrated the LUV membrane. In contrast, **MT6-Cr2** at a high concentration of 10 μM showed extra DLS peaks at ~600 and 1000 nm, but not at lower concentrations. This result agrees well with the naked eye observation, showing no visible precipitates at up to 7.5 μM. Thus, undoubtedly, **MT6-Cr1** and **MT6-Cr2** could insert readily into the LUV membrane lipid bilayer at concentrations up to 7.5 μM but unable

DOI: 10.31635/ccschem.020.202000475
Citation: *CCS Chem.* **2020**, 2, 2269–2279
Citation denotes calendar and volume year of first online publication.
Issue Assignment: Volume 3 (2021), Issue 8

to transport the alkali metal ions across the membrane. Such inactivity also confirms the limited contribution (if any) from the possible molecular tumbling of the **MT**s in the lipid bilayer to convey ions across.

Second, the swing-relay ion transport mechanism should also dictate some synergistic effects among the four flexible arms. We verified this effect by fabricating another membrane-span control compound, **MT6-Cr3**, which only possessed two operational arms, with the other two arms terminated merely by a methyl group. We compared **MT6-Cr3** with **MT6-C10** that had all four arms (Figure 2). Using the Hill analysis, the $EC_{50}(K^+)$ value of **MT6-Cr3** was determined to be 4.6 μM (Figure 2 and Supporting Information Figure S16), an activity deemed only at ~20% of **MT6-C10** [$EC_{50}(K^+) = 0.9$ μM]. This large difference in activity indicated that the four arms in **MT6-C10** worked synergistically via either creating more ion-relay pathways among the four crown units or two of the four crown units provided the anchoring effect, while the other two engaged in swing-relay action. Interestingly, when we used the R_{K^+}/R_{Na^+} ratio to quantify the K^+/Na^+ selectivity of **MT6-Cr3**, we obtained a value of 3.4 (see Supporting Information Figure S17), almost identical to that of **MT6-C10**.

Third, by judging from the **MT**'s physical dimension, we envisioned that there could exist another possible yet energetically less favorable ion transport mechanism; namely, the nonrelaying swing-only action, wherein a single-arm carries the ion across the entire membrane. We tested this hypothesis by preparing **MT6-Cr4** with a similar physical size as **MT6-C10**, but with three out of the four ion-binding 18-crown-6 units replaced by indolyl groups (Figure 2), followed by quantification of the **MT6-Cr4** effect. Like crowns, these indolyl groups tended to localize at the membrane–water interfaces as lipid anchors by virtue of hydrogen bonding with the lipid carbonyl groups and cation–π interactions,[42] with their ion affinity much lower than the crowns. As a result, any ion transport activity observed on **MT6-Cr4** should only be ascribed to the nonrelaying swing-only action of the single crown ether-containing operational arm. Experimentally, the $EC_{50}(K^+)$ of **MT6-Cr4** was determined to be 28.5 μM using the Hill analysis (Figure 2 and Supporting Information Figure S19). Thus, the EC_{50} value of **MT6-Cr4** is >30 times higher than that of **MT6-C10** [$EC_{50}(K^+) =$ 0.9 μM], indicating that **MT6-Cr4** had a much weaker transporter activity. In contrast, we prepared another comparative control, **MT6-Cr5**, containing two ion-binding crown units and two lipid anchoring-indolyl groups that showed a much higher ion transport activity [$EC_{50}(K^+) = 1.4$ μM, Figure 2] than the single-crown **MT6-Cr4**. Besides, a commercially available small molecule compound **Benzo-18-Crown-6** was purchased from Sigma and measured for its ion transport performance using the HPTS assay. As expected, it preferably transported K^+ over other alkali metal ions (Supporting Information Figure S23). The K^+ transport EC_{50} value is determined to be 43.9 μM, which is about 1.5 times that of **MT6-Cr4** containing a single crown arm. This implied that the single crown unit in **MT6-Cr4** is not simply acting as an isolated ion carrier. Overall, these observations confirmed the negligible contribution of the nonrelaying swing-only action in the overall ion transport activity of these **MT**s. They also demonstrated highly efficient ion transport capability, especially for **MT6-C10**, to be dominated by the unconventional two-station swing-relay mechanism depicted in Figure 1d. Also, it is evident that while two crown units were in the swing-relay action, the anchoring effect of the other two flexible arms played a positive role in promoting overall ion transport performance. This inference is drawn from the comparison of the transport activities between **MT6-Cr3** and **MT6-Cr5** [$EC_{50}(K^+) = 4.6$ μM vs. 1.4 μM] wherein the only structural difference is the two lipid-anchoring indolyl groups (Figure 2).

Further, the transport rate between K^+ and H^+ ions for the most active **MT6-C10** was compared by introducing carbonyl cyanide-*p*-trifluoromethoxyphenylhydrazone (FCCP) as the proton carrier in the HPTS assay. If the efflux rate of H^+ is far lower than the influx of K^+ ion for a LUV, the presence of FCCP should promote overall ion transport efficiency by accelerating the H^+ transport to nearer or to be parallel with that of K^+. As shown

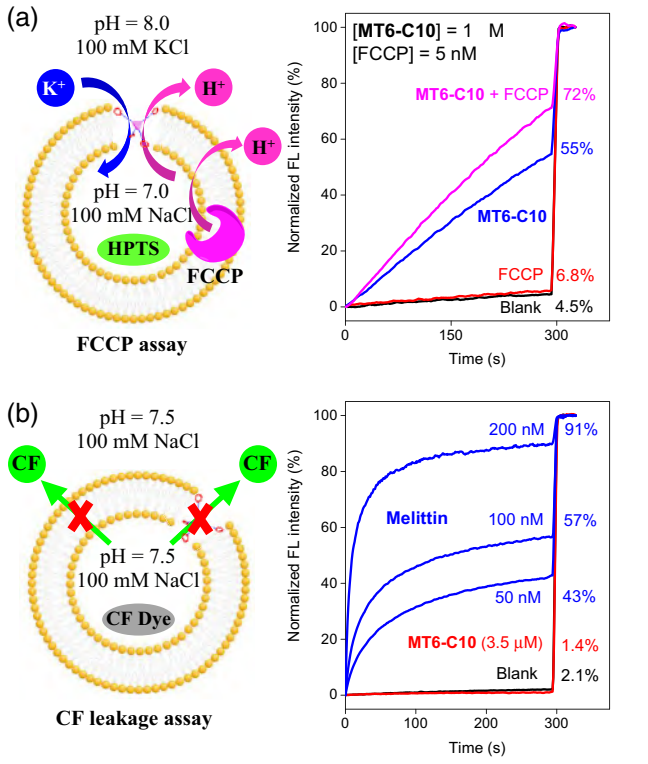

Figure 4 | *(a) FCCP assay compares the transport rate of K^+ and H^+ or OH^-. (b) 5(6)-carboxyfluorescein leakage assay to confirm the LUV integrity in the presence of **MT6-C10**. FCCP, carbonyl cyanide-*p*-trifluoromethoxyphenylhydrazone; LUV, large unilamellar vesicle.*

DOI: 10.31635/ccschem.020.202000475
Citation: *CCS Chem.* **2020**, 2, 2269–2279
Citation denotes calendar and volume year of first online publication.
Issue Assignment: Volume 3 (2021), Issue 8

in Figure 4a, FCCP alone at 5 nM induced negligible fluorescence enhancement (2.3%), compared with the blank, whereas a significant increase in fluorescence intensity of 17% was observed with the transport activity of **MT6-C10** alone (1 μM, 55%) and much higher intensity in the presence of 5 nM FCCP (72%). This data unambiguously confirmed that **MT6-C10**-mediated transport of K^+ ions was much faster than that of H^+ or OH^- across the membrane.

The carboxyfluorescein (CF) dye leakage assay (Supporting Information Figure S24) was also conducted to verify the LUV membrane integrity in the presence of **MT6-C10**. In this assay, the self-quenching CF dye at a high concentration of 50 mM was encapsulated inside the EYPC-based LUVs, and most of the CF dye molecules remained as nonfluorescent dimers under this condition. A dramatic CF fluorescence increase was expected if any CF dye leakage from the LUV or any membrane destruction occurred. As shown in Figure 4b, at 3.5 μM that gives 100% R_{K^+} in the HPTS assay, **MT6-C10** induced no fluorescence change at all. In sharp contrast, the melittin positive control in this assay caused a significant CF fluorescence increase of 43–91% at concentrations ranging from 50 to 200 nM, as it could form membrane pores of larger size than the CF dye molecules or even a complete LUV membrane lysate. Together with the fact that structurally similar **MT5**s are weakly active (Figure 3b), this contradistinctive data showed that the integrity of LUV membranes in the presence of **MT6-C10** and the ion transport activities observed indeed resulted from transmembrane K^+ ion transport, instead of any **MT**-induced membrane-lysing effects.

As a final remark, the swing-relay mechanism exhibited by these **MT**s shared some similarities but not precisely the same as either the channel- or carrier-facilitated conventional ion transport paradigms. Resembling channels, these **MT**s are open to both the intra- and extravesicular regions simultaneously, whereas, like carriers, the operational tetrahedron arms are free to move in the bilayer membrane, and consequently, the ion transport might not follow any predefined pathways.[43] Single-channel current measurements were, therefore, conducted on the most active **MT6-C10** to determine which mechanism (carrier or channel) was more akin to the **MT**s-mediated swing-relay model. The failure of capturing any single-current signals after extensive efforts suggested that these **MT**s function more like ion carriers.

Conclusion

We have demonstrated a novel class of crown ether-appended **MT**s containing mobile arms as highly active transmembrane ion transporters. As elucidated, the presence of multiple ion-capturing and ion-relaying crown units, along with supporting mobile arms, facilitated an unconventional two-station swing-relay mechanism, whose performance was mostly dependent on the choice of crown ethers, and to a lesser degree, length of mobile arms. **MT**s containing 15-crown-5 are mostly Na^+ selective but only weakly active. Highly active and K^+-selective ion transport was typically observed for all 18-crown-6-containing **MT**s, with the highest activity achieved by **MT6-C10** [$EC_{50}(K^+) = 0.9$ μM or 0.9 mol % relative to lipid] and the highest K^+/Na^+ selectivity of 6.3 on **MT6-C4**. The essential roles of flexible linkers' flexibility are synergistic effect among the mobile operational arms and negligible contribution of the nonrelaying swing-only action in the overall ion transport activity, which were also demonstrated experimentally. We believe that the novel swing-relay mechanism, structural modularity, and facile synthesis of these ion-transporting **MT**s could stimulate further development of mobile arm-containing hexahedrons, octahedrons, and other higher-order transporters, not only for scientific advances but also toward practical applications in the future.

Supporting Information

Supporting Information is available.

Conflict of Interest

There is no conflict of interest to report.

Funding Information

This work was supported by Northwestern Polytechnical University and the NanoBio Lab (Biomedical Research Council, Agency for Science, Technology, and Research).

References

1. Zaydman, M. A.; Silva, J. R.; Cui, J. Ion Channel Associated Diseases: Overview of Molecular Mechanisms. *Chem. Rev.* **2012**, *112*, 6319–6333.
2. Cooper, E. C.; Jan, L. Y. Ion Channel Genes and Human Neurological Disease: Recent Progress, Prospects, and Challenges. *Proc. Natl. Acad. Sci. U. S. A.* **1999**, *96*, 4759.
3. Chew, T. A.; Orlando, B. J.; Zhang, J.; Latorraca, N. R.; Wang, A.; Hollingsworth, S. A.; Chen, D.-H.; Dror, R. O.; Liao, M.; Feng, L. Structure and Mechanism of the Cation–Chloride Cotransporter NKCC1. *Nature* **2019**, *572*, 488–492.
4. Mahendran, K. R.; Niitsu, A.; Kong, L.; Thomson, A. R.; Sessions, R. B.; Woolfson, D. N.; Bayley, H. A Monodisperse Transmembrane α-Helical Peptide Barrel. *Nat. Chem.* **2016**, *9*, 411.
5. Muraglia, K. A.; Chorghade, R. S.; Kim, B. R.; Tang, X. X.; Shah, V. S.; Grillo, A. S.; Daniels, P. N.; Cioffi, A. G.; Karp, P. H.; Zhu, L.; Welsh, M. J.; Burke, M. D. Small-Molecule Ion Channels Increase Host Defences in Cystic Fibrosis Airway Epithelia. *Nature* **2019**, *567*, 405–408.

6. Bertholet, A. M.; Chouchani, E. T.; Kazak, L.; Angelin, A.; Fedorenko, A.; Long, J. Z.; Vidoni, S.; Garrity, R.; Cho, J.; Terada, N.; Wallace, D. C.; Spiegelman, B. M.; Kirichok, Y. H+ Transport Is an Integral Function of the Mitochondrial ADP/ATP Carrier. *Nature* **2019**, *571*, 515–520.
7. Ren, C. L.; Zeng, F.; Shen, J.; Chen, F.; Roy, A.; Zhou, S. Y.; Ren, H. S.; Zeng, H. Q. Pore-Forming Monopeptides as Exceptionally Active Anion Channels. *J. Am. Chem. Soc.* **2018**, *140*, 8817–8826.
8. Zeng, F.; Liu, F.; Yuan, L.; Zhou, S. Y.; Shen, J.; Li, N.; Ren, H. S.; Zeng, H. Q. A Pore-Forming Tripeptide as an Extraordinarily Active Anion Channel. *Org. Lett.* **2019**, *21*, 4826–4830.
9. Davis, J. T.; Okunola, O.; Quesada, R. Recent Advances in the Transmembrane Transport of Anions. *Chem. Soc. Rev.* **2010**, *39*, 3843–3862.
10. Brotherhood, P. R.; Davis, A. P. Steroid-Based Anion Receptors and Transporters. *Chem. Soc. Rev.* **2010**, *39*, 3633–3647.
11. Kim, D. S.; Sessler, J. L. Calix[4]pyrroles: Versatile Molecular Containers with Ion Transport, Recognition, and Molecular Switching Functions. *Chem. Soc. Rev.* **2015**, *44*, 532–546.
12. Benz, S.; Macchione, M.; Verolet, Q.; Mareda, J.; Sakai, N.; Matile, S. Anion Transport with Chalcogen Bonds. *J. Am. Chem. Soc.* **2016**, *138*, 9093–9096.
13. Gale, P. A.; Davis, J. T.; Quesada, R. Anion Transport and Supramolecular Medicinal Chemistry. *Chem. Soc. Rev.* **2017**, *46*, 2497–2519.
14. Matile, S.; Vargas Jentzsch, A.; Montenegro, J.; Fin, A. Recent Synthetic Transport Systems. *Chem. Soc. Rev.* **2011**, *40*, 2453–2474.
15. Vargas Jentzsch, A.; Hennig, A.; Mareda, J.; Matile, S. Synthetic Ion Transporters that Work with Anion–π Interactions, Halogen Bonds, and Anion–Macrodipole Interactions. *Acc. Chem. Res* **2013**, *46*, 2791–2800.
16. Montenegro, J.; Ghadiri, M. R.; Granja, J. R. Ion Channel Models Based on Self-Assembling Cyclic Peptide Nanotubes. *Acc. Chem. Res.* **2013**, *46*, 2955–2965.
17. Fyles, T. M. How Do Amphiphiles Form Ion-Conducting Channels in Membranes? Lessons from Linear Oligoesters. *Acc. Chem. Res.* **2013**, *46*, 2847–2855.
18. Otis, F.; Auger, M.; Voyer, N. Exploiting Peptide Nanostructures to Construct Functional Artificial Ion Channels. *Acc. Chem. Res.* **2013**, *46*, 2934–2943.
19. Gokel, G. W.; Negin, S. Synthetic Ion Channels: From Pores to Biological Applications. *Acc. Chem. Res.* **2013**, *46*, 2824–2833.
20. Barboiu, M.; Gilles, A. From Natural to Bioassisted and Biomimetic Artificial Water Channel Systems. *Acc. Chem. Res.* **2013**, *46*, 2814–2823.
21. Gong, B.; Shao, Z. Self-Assembling Organic Nanotubes with Precisely Defined, Sub-Nanometer Pores: Formation and Mass Transport Characteristics. *Acc. Chem. Res.* **2013**, *46*, 2856–2866.
22. Si, W.; Xin, P.; Li, Z.-T.; Hou, J.-L. Tubular Unimolecular Transmembrane Channels: Construction Strategy and Transport Activities. *Acc. Chem. Res.* **2015**, *48*, 1612–1619.
23. Huo, Y.; Zeng, H. "Sticky"-Ends-Guided Creation of Functional Hollow Nanopores for Guest Encapsulation and Water Transport. *Acc. Chem. Res.* **2016**, *49*, 922–930.
24. Chen, J.-Y.; Hou, J.-L. Controllable Synthetic Ion Channels. *Org. Chem. Front.* **2018**, *5*, 1728–1736.
25. Malla, J. A.; Umesh, R. M.; Yousf, S.; Mane, S.; Sharma, S.; Lahiri, M.; Talukdar, P. A Glutathione Activatable Ion Channel Induces Apoptosis in Cancer Cells by Depleting Intracellular Glutathione Levels. *Angew. Chem. Int. Ed.* **2020**, *59*, 7944–7952.
26. McNally, B. A.; O'Neil, E. J.; Nguyen, A.; Smith, B. D. Membrane Transporters for Anions that Use a Relay Mechanism. *J. Am. Chem. Soc.* **2008**, *130*, 17274–17275.
27. Chen, S.; Wang, Y.; Nie, T.; Bao, C.; Wang, C.; Xu, T.; Lin, Q.; Qu, D.-H.; Gong, X.; Yang, Y.; Zhu, L.; Tian, H. An Artificial Molecular Shuttle Operates in Lipid Bilayers for Ion Transport. *J. Am. Chem. Soc.* **2018**, *140*, 17992–17998.
28. Ren, C. L.; Chen, F.; Ye, R. J.; Ong, Y. S.; Lu, H. F.; Lee, S. S.; Ying, J. Y.; Zeng, H. Q. Molecular Swings as Highly Active Ion Transporters. *Angew. Chem. Int. Ed.* **2019**, *58*, 8034–8038.
29. Ye, R. J.; Ren, C. L.; Shen, J.; Li, N.; Chen, F.; Roy, A.; Zeng, H. Q. Molecular Ion Fishers as Highly Active and Exceptionally Selective K+ Transporters. *J. Am. Chem. Soc.* **2019**, *141*, 9788–9792.
30. Weiss, L. A.; Sakai, N.; Ghebremariam, B.; Ni, C.; Matile, S. Rigid Rod-Shaped Polyols: Functional Nonpeptide Models for Transmembrane Proton Channels. *J. Am. Chem. Soc.* **1997**, *119*, 12142–12149.
31. Hall, C. D.; Kirkovits, J. G.; Hall, C. A. Towards a Redox-Active Artificial Ion Channel. *Chem. Commun.* **1999**, 1897–1898.
32. Sakai, N.; Gerard, D.; Matile, S. Electrostatics of Cell Membrane Recognition: Structure and Activity of Neutral and Cationic Rigid Push-Pull Rods in Isoelectric, Anionic, and Polarized Lipid Bilayer Membranes. *J. Am. Chem. Soc.* **2001**, *123*, 2517–2524.
33. Gokel, G. W.; Mukhopadhyay, A. Synthetic Models of Cation-Conducting Channels. *Chem. Soc. Rev.* **2001**, *30*, 274–286.
34. Sun, Z.; Barboiu, M.; Legrand, Y.-M.; Petit, E.; Rotaru, A. Highly Selective Artificial Cholesteryl Crown Ether K+-Channels. *Angew. Chem. Int. Ed.* **2015**, *127*, 14681–14685.
35. Gilles, A.; Barboiu, M. Highly Selective Artificial K+ Channels: An Example of Selectivity-Induced Transmembrane Potential. *J. Am. Chem. Soc.* **2016**, *138*, 426–432.
36. Ren, C.; Shen, J.; Zeng, H. Combinatorial Evolution of Fast-Conducting Highly Selective K+-Channels via Modularly Tunable Directional Assembly of Crown Ethers. *J. Am. Chem. Soc.* **2017**, *139*, 12338–12341.
37. Ren, C.; Ding, X.; Roy, A.; Shen, J.; Zhou, S.; Chen, F.; Yau Li, S. F.; Ren, H.; Yang, Y. Y.; Zeng, H. A Halogen Bond-Mediated Highly Active Artificial Chloride Channel with High Anticancer Activity. *Chem. Sci.* **2018**, *9*, 4044–4051.
38. More, M. B.; Ray, D.; Armentrout, P. B. Intrinsic Affinities of Alkali Cations for 15-Crown-5 and 18-Crown-6: Bond Dissociation Energies of Gas-Phase M^+–Crown Ether Complexes. *J. Am. Chem. Soc.* **1999**, *121*, 417–423.

DOI: 10.31635/ccschem.020.202000475
Citation: *CCS Chem.* **2020**, 2, 2269–2279
Citation denotes calendar and volume year of first online publication.
Issue Assignment: Volume 3 (2021), Issue 8

39. Guo, X.; Zhu, Y.; Wei, M.; Wu, X.; Lü, L.; Lu, X. Theoretical Study of Hydration Effects on the Selectivity of 18-Crown-6 Between K^+ and Na^+. *Chin. J. Chem. Engin.* **2011**, *19*, 212–216.
40. Eisenman, G.; Horn, R. Ionic Selectivity Revisited: The Role of Kinetic and Equilibrium Processes in Ion Permeation Through Channels. *J. Membr. Biol.* **1983**, *76*, 197–225.
41. Zeng, L. Z.; Zhang, H.; Wang, T.; Li, T. Enhancing K+ Transport Activity and Selectivity of Synthetic K^+ Channels via Electron-Donating Effects. *Chem. Commun.* **2020**, *56*, 1211–1214.
42. Norman, K. E.; Nymeyer, H. Indole Localization in Lipid Membranes Revealed by Molecular Simulation. *Biophys. J.* **2006**, *91*, **2046**.
43. Gouaux, E.; MacKinnon, R. Principles of Selective Ion Transport in Channels and Pumps. *Science* **2005**, *310*, 1461.

DOI: 10.31635/ccschem.020.202000475
Citation: *CCS Chem.* **2020**, 2, 2269–2279
Citation denotes calendar and volume year of first online publication.
Issue Assignment: Volume 3 (2021), Issue 8